

Non-Doped Deep Blue and Doped White Electroluminescence Devices Based on Phenanthroimidazole Derivative

Shuo Chen¹ · Yukun Wu² · Shoucheng Hu² · Yi Zhao² · Daining Fang^{1,3}

Received: 19 August 2016 / Accepted: 3 November 2016 / Published online: 29 November 2016
© Springer Science+Business Media New York 2016

Abstract A novel deep-blue emitter **PhImPOTD** based on phenanthroimidazole was synthesized, which is incorporated by an electron-donating dibenzothiophene unit and electron-withdrawing phenanthroimidazole and diphenylphosphine oxide moieties. Furthermore, the weak π - π stacking and intermolecular aggregation render the photoluminescence quantum yield is as high as 0.34 in the solid state. Non-doped organic light emitting diodes (OLEDs) based on **PhImPOTD** emitter exhibits a low turn-on voltage of 3.6 V, a favorable efficiency of 1.13 cd A⁻¹ and a deep blue emission with Commission Internationale de l'Éclairage (CIE) coordinates of (0.15, 0.08). The CIE is very close to the NTSC (National Television Standards Committee) blue standard (CIE: 0.14, 0.08). **PhImPOTD** is also utilized as blue emitter and the host for a yellow emitter (PO-01) to fabricate white organic light-emitting diodes (WOLEDs). This

gives a forward-viewing maximum CE of 4.83 cd A⁻¹ and CIE coordinates of (0.32, 0.32) at the luminance of 1000 cd m⁻². Moreover, the single-carrier devices unambiguously demonstrate that typical bipolar-dominant characteristics of **PhImPOTD**. This work demonstrates not only that the phenanthroimidazole unit is an excellent building block to construct deep blue emission materials, but also the introduction of a diphenylphosphine oxide deprotonation substituent is an efficient tactic for harvesting deep-blue emitting devices.

Keywords OLEDs · Phenanthroimidazole derivative · Bipolar · Non-doped deep blue · Doped white

Introduction

In the field of consumer electronics, organic light-emitting diodes (OLEDs) as solid-state lighting are progressively replacing the traditional display technology due to their superior lightweight, flexible and large viewing angle [1, 2]. Among diverse design strategies, the properties of three essential emitting elements (red, green and blue) are directly influence the performance of devices [3–5]. After decades of development, several excellent green and red emitting molecules have been designed and applied successfully to improve to the light emitting capability of OLEDs [6]. However, the overall performance and stability of blue (especially deep blue) fluorescence emitters and devices are still inferior to those red and green counterparts [7, 8]. The blue emitter can not only effectively reduce power consumption of the devices but also be utilized to generate light of other colors by energy cascade to lower energy fluorescent or phosphorescent dopants. To date, the marketable OLEDs mainly adopt the doped host-guest emitting layer.

Shuo Chen and Yukun Wu These authors contributed equally.

Electronic supplementary material The online version of this article (doi:10.1007/s10895-016-1970-5) contains supplementary material, which is available to authorized users.

✉ Daining Fang
fangdn@pku.edu.cn

¹ State Key Laboratory for Turbulence and Complex System, College of Engineering, Peking University, Chengfu Road, Haidian District, Beijing 100871, People's Republic of China

² State Key Laboratory on Integrated Optoelectronics, College of Electronics Science and Engineering, Jilin University, 2699 Qianjin Street, Changchun 130012, People's Republic of China

³ Institute of Advanced Structure Technology, Beijing Institute of Technology, South Street No. 5, Zhongguancun, Haidian District, Beijing 100081, People's Republic of China

Nevertheless, the generally used heavy metals for phosphorescence are confined to iridium (Ir) and platinum (Pt) [9–11], which are rather expensive and dependent on limited global resources. Thus, organic molecule with free heavy-metal containing meets the eco-friendly theme [12]. At the same time, phosphorescent materials also suffer from the lack of deep blue emitters and their inherent short lifetimes when utilized to configure white organic light-emitting diodes (WOLEDs) [13]. Therefore, the development of high-performance deep-blue emitting OLEDs (CIE criterion: $y < 0.15$ and $x + y < 0.30$) and related materials is still a challenging issue [14, 15]. In order to realize the deep blue emission, the strategic molecular design should be focus on relatively short conjugation and weak intermolecular aggregation [16]. Also, the electron affinities of blue-emitting materials should be increased to realize balanced charge injection and transport, since the electron injection and transport ability in organic semiconductors is relatively low compared to that of hole [17, 18]. The *n*-type phenanthroimidazole (PI) derivatives always adopt less conjugative configuration such as the twisted linkage or non-conjugative linkage [19–22]. The PI moiety as the core structure linked with a freely rotatable benzene ring and end-capsulated with donor units is the representative donor– π –acceptor dipolar molecule [23–27]. In our molecule **PhImPOTD**, electron-deficiency diphenylphosphine oxide is bonding with NH site at the imidazole ring, which could effectively inhibit molecular aggregation, π – π stacking and even fluorescence quenching in the solid state. It is noted that diphenylphosphine oxide unit, in contrast with the electron-rich group, also affords a hypsochromic shift function of emission to ensure the deep blue emitting OLEDs [28].

In this work, we report a triple twisted PI derivative, which is designed based on donor– π –acceptor approach and utilized phenyl bridge to concatenate two planar electron-transporting PI and hole-transporting dibenzothiophene (TD) units. In this way, such bipolar feature is beneficial to charge transport and balancing for obtaining high-efficiency devices in comparison with conventional unipolar materials. In addition, diphenylphosphine oxide is employed to construct multi-dimension framework by deprotonation on the site of imidazole. Therefore, the yielding sterically hindered and highly twisted molecular configuration is benefit to increase the photoluminescence quantum yield. Thermal, photophysical, and electroluminescent properties of the deep blue emitting **PhImPOTD** are comprehensively investigated. Hybrid WOLEDs, combining blue fluorophores and yellow phosphors, has been fabricated and investigated. It is approved that **PhImPOTD** possesses high luminescent efficiency, excellent luminous/thermo-stability and balanced charge carrier injection and transport, which has opened us new avenues for designing deep blue PI derivatives for high-performance OLEDs.

Experimental

Materials and Instruments

All the reagents and solvents used for the synthesis of the **PhImPOTD** were purchased from Aldrich, J&K and TCI companies and used as received. Dopant material PO-01 was purchased from Lumtec Corp. (taiwan). ^1H magnetic resonance (NMR) spectra were recorded using a Bruker AVANCE III 500-MHz spectrometer, using CDCl_3 as the solvent and tetramethylsilane (TMS) as the internal standard. High resolution mass spectra were recorded on a Bruker APEX IV fourier transform ion cyclotron resonance mass spectrometer. Elemental analysis for C, H, N and S were performed on a Elementar Analysensysteme GmbH. All manipulations involving air-sensitive reagents were performed in an atmosphere of dry Ar. Absorption and photoluminescence (PL) emission spectra of the target compound were measured using a Perkin Elmer Lambda-750 UV-Vis-NIR spectrophotometer and LS 55 fluorescence spectrometer, respectively. The luminescence quantum yield of compound was measured at room temperature and cited relative to a reference solution of 9,10-diphenylanthracene ($\Phi = 0.9$ in cyclohexane) as a standard, and they were calculated according to the well-known equation:

$$\frac{\varphi_{\text{overall}}}{\varphi_{\text{ref}}} = \left(\frac{n}{n_{\text{ref}}} \right)^2 \frac{A_{\text{ref}}}{A} \frac{I}{I_{\text{ref}}} \quad (1)$$

In Eq. (1), n , A , and I denote the refractive index of solvent, the area of the emission spectrum, and the absorbance at the excitation wavelength, respectively, and φ_{ref} represents the quantum yield of the standard 9,10-diphenylanthracene solution. The subscript *ref.* denotes the reference, and the absence of a subscript implies an unknown sample. For the determination of the quantum yield, the excitation wavelength was chosen so that $A < 0.05$. For the solid samples, the quantum yield for the compound was determined at room temperature through an absolute method using an Edinburgh Instruments' integrating sphere coupled to a modular Edinburgh FLS 920 fluorescence spectrophotometer. The values reported are the average of three independent determinations for each sample. The absolute quantum yield was calculated using the following expression:

$$\Phi = \frac{\int L_{\text{emission}}}{\int L_{\text{reference}} - \int L_{\text{sample}}} \quad (2)$$

In expression (2), L_{emission} is the emission spectrum of the sample, collected using the sphere, E_{sample} is the spectrum of

the incident light used to excite the sample, collected using the sphere, and $E_{\text{reference}}$ is the spectrum of the light used for excitation with only the reference in the sphere. The method is accurate to within 10%. Thermogravimetric analysis (TGA) and differential scanning calorimetry (DSC) were performed on Perkin Elmer TGA 4000 and DSC 8000 thermal analyzers under nitrogen atmosphere at a heating rate of $10\text{ }^{\circ}\text{C min}^{-1}$. Cyclic voltammetric (CV) measurements were carried out in a conventional three electrode cell using a Pt button working electrode of 2 mm in diameter, a platinum wire counter electrode, and a saturated calomel electrode (SCE) reference electrode on a computer-controlled CHI660d electrochemical workstation at room temperature. Reduction CV of the compound was performed in CH_2Cl_2 containing tetrabutylammonium hexafluorophosphate (Bu_4NPF_6 , 0.1 M) as the supporting electrolyte. Ferrocene was used as an external standard. Electrochemistry was done at a scan rate of 100 mV s^{-1} .

Computational Details

The theoretical investigation of geometry optimization was performed with the *Gaussian 09* program package [29]. Density functional theory (DFT) was calculated at Beck's three-parameter hybrid exchange functional [30] and Lee, and Yang and Parr correlation functional [31] B3LYP/6-31G (d). The spin density distributions were visualized using *Gaussview 5.0.8*.

Device Fabrication and Measurement

Prior to the device fabrication, the patterned ITO-coated glass substrates were scrubbed and sonicated consecutively with detergent water, deionized water, and acetone, dried in drying cabinet, and then exposed to a UV-ozone environment for 30 min. After these processes, the substrates were transferred into a vacuum chamber for sequential deposition of all the organic layers by thermally evaporation with a base pressure ($\sim 4.0 \times 10^{-4}$ Pa) at a rate of $0.1\text{--}0.2\text{ nm s}^{-1}$ monitored in situ with the quartz oscillator. LiF covered by Al is used as cathode without breaking the vacuum. All the samples were measured directly after fabrication without encapsulation at room temperature under ambient atmosphere. The current-voltage-luminance characteristics were carried out using a PR655 Spectrascan spectrometer and a Keithley 2400 programmable voltage-current source. The external quantum efficiency (EQE) and luminous efficiency (LE) were calculated assuming Lambertian distribution, and then calibrated to the efficiencies obtained at 1000 cd m^{-2} in the integrating sphere (Jm-3200). The configurations of Device A was ITO/MoO₃ (10 nm)/NPB (80 nm)/PhImPOTD (30 nm)/TPBi (40 nm)/LiF (1 nm)/Al (100 nm). The nominal hole-only and electron-only devices were fabricated with the configurations of ITO/MoO₃

(0.2 nm)/NPB (40 nm)/PhImPOTD (30 nm)/NPB (40 nm)/MoO₃ (0.2 nm)/Al (100 nm) (hole-only transporting Device) and ITO (100 nm)/LiF (0.1 nm)/TPBi (40 nm)/PhImPOTD (30 nm)/TPBi (40 nm)/LiF (0.1 nm)/Al (100 nm) (electron-only transporting Device). The doped WOLEDs device B was fabricated with the structure ITO/MoO₃ (0.2 nm)/NPB (40 nm)/PhImPOTD (15 nm)/PO-01 (0.2 nm)/PhImPOTD (15 nm)/TPBi (40 nm)/LiF (0.1 nm)/Al.

Synthesis

Synthesis of Dibenzothiophene-4-Dioxaborolane (TD4B)

TD4B was synthesized according to the literature procedures [28]. Yield: 80%. ¹H NMR (TMS, CDCl₃, 500 MHz): ppm $\delta = 8.22$ (d, $J = 8.0$ Hz, 1 H), 8.11 (t, $J = 6.5$ Hz, 2 H), 8.90 (d, $J = 7.5$ Hz, 1 H), 7.84 (t, $J = 4.0$ Hz, 1 H), 7.45–7.40 (m, 3 H), 1.35 (s, 12 H); HR-ESI-MS: $[\text{M} + \text{H}]^+$ m/z calcd for C₁₈H₂₀BO₂S: 311.12797, found: 311.12748; elemental analysis calcd (%) for C₁₈H₁₉BO₂S: C 69.69, H 6.17, N 10.31, S 10.33; found: C 69.58, H 6.11, N 10.45, S 10.42.

Synthesis of 4-(Diphenylphosphinyl)Benzenamine (POBA)

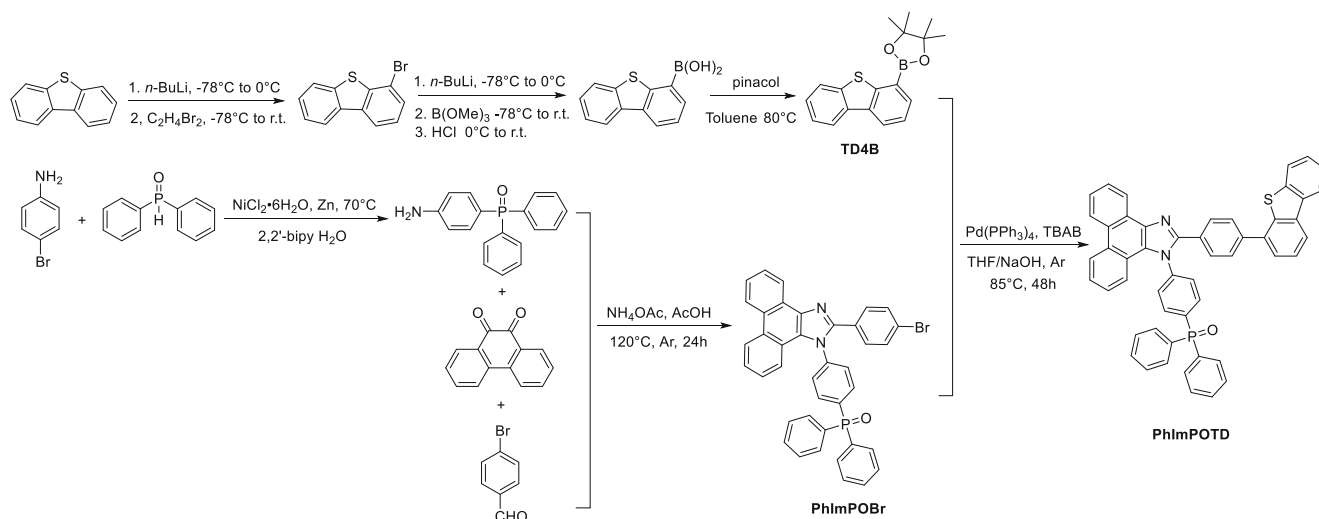
To a 100 mL round bottom flask fitted with magnetic bar, was added NiCl₂·6H₂O (23.6 mg, 0.1 mmol), zinc (127.9 mg, 2.0 mmol), 2,2'-bipyridine (bpy) (31.2 mg, 0.2 mmol), 4-bromoaniline (206.4 mg, 1.2 mmol), diphenylphosphine oxide (202.1 mg, 1.0 mmol) and water (15 mL). The reaction mixture was then stirred at 70 °C for 24 h. After completion of the reaction, the mixture was allowed to cool to room temperature and added with CH₂Cl₂ and water. The organic layer was isolated and the remaining aqueous phase was further extracted with CH₂Cl₂ (10 mL × 3). Then the organic phases were combined and dried with anhydrous MgSO₄, and purified by silica gel column chromatography using CH₂Cl₂/MeOH (15:1) as the eluent to afford a white powder. Yield: 75%. ¹H NMR (TMS, CDCl₃, 500 MHz): ppm $\delta = 7.59\text{--}7.5$ (m, 6 H), 7.52–7.48 (m, 4 H), 7.21–7.17 (m, 2 H), 6.63 (dd, $J = 6.0, 2.5$ Hz, 2 H), 5.79 (br s, 2 H); HR-ESI-MS: $[\text{M} + \text{H}]^+$ m/z calcd for C₁₈H₁₇NOP: 294.10423, found: 294.10422; elemental analysis calcd (%) for C₄₀H₂₆N₂O₂: C 84.78, H 4.62, N 4.94; found: C 84.68, H 4.71, N 4.86.

Synthesis of 2-(4-Bromophenyl)

-1-(4-Diphenylphosphinylphenyl)

-1H-Phenanthro[9,10-d]imidazole (PhImPOBr)

A mixture of 4-bromobenzaldehyde (92.0 mg, 0.5 mmol), phenanthrene-9,10-dione (104.0 mg, 0.5 mmol), 4-(diphenylphosphinyl)benzenamine (732.8 mg, 2.5 mmol),



Scheme 1 Synthetic pathways toward bipolar molecule **PhImPOTD**

ammonium acetate (130.1 mg, 2.0 mmol), and acetic acid (30 mL) were refluxed under nitrogen in an oil bath. After 24 h, the mixture was cooled and concentrated under reduced pressure, the crude product was extracted by CH₂Cl₂/H₂O. It was then purified by chromatography using CH₂Cl₂/MeOH (15:1) as an eluent to obtain the product as yellow powder. Yield: 62%. ¹H NMR (TMS, CDCl₃, 500 MHz): ppm δ = 7.21 (d, *J* = 8.0 Hz, 1H), 7.30 (t, *J* = 7.5 Hz, 1H), 7.39 (d, *J* = 8.5 Hz, 2H), 7.44 (d, *J* = 8.5 Hz, 2H), 7.53–7.55 (m, 5H), 7.60–7.68 (m, 5H), 7.70–7.75 (m, 5H), 7.91 (dd, *J* = 8.0 Hz, 2H), 8.70 (d, *J* = 8.5 Hz, 1H), 8.78 (d, *J* = 8.0 Hz, 1H), 8.8 (d, *J* = 9.0 Hz, 1H); HR-ESI-MS: [M + H]⁺ *m/z* calcd for C₃₉H₂₇BrN₂OP: 649.10389, found: 649.10200; elemental analysis calcd (%) for C₃₉H₂₆BrN₂OP: C 72.12 H 4.03, N 4.31; found: C 72.18, H 4.13, N 4.43.

Synthesis of 2-(4-Dibenzothiophene Sulfone)-1-(4-Diphenylphosphinylphenyl)-1H-Phenanthro[9,10-d]imidazole (PhImPOTD)

A mixture of **PhImPOBr** (974.3 mg, 1.5 mmol), **TD4B** (465.3 mg, 1.5 mmol), tetrakis(triphenylphosphine)palladium (173.3 mg, 0.15 mmol), tetrabutylammonium bromide (48.5 mg, 0.15 mmol), and aqueous solution of sodium hydroxide (2 mol L⁻¹, 9 mmol) in THF (20 mL) was stirred under argon at 80 °C for 48 h. After quenched with aqueous NH₄Cl solution, the mixture was extracted with CH₂Cl₂. The combined organic extracts were washed with brine and dried over anhydrous MgSO₄. After removing the solvent, the residue was purified by column chromatography on silica gel using ethyl acetate as the eluent to give a white powder. Yield: 64%. ¹H NMR (TMS, CDCl₃, 500 MHz): ppm δ = 7.35 (t, *J* = 8.5 Hz, 1H), 7.47–7.63 (m, 12H), 7.68–7.84 (m, 13H), 7.98 (t, *J* = 8.5 Hz, 2H), 8.23 (t, *J* = 7.0 Hz, 2H),

8.75 (d, *J* = 8.5 Hz, 1H), 8.83 (d, *J* = 8.5 Hz, 1H), 8.92 (d, *J* = 8.0 Hz, 1H); HR-ESI-MS: [M + H]⁺ *m/z* calcd for C₅₁H₃₄N₂OPS: 753.21240, found: 753.21298; elemental analysis calcd (%) for C₅₁H₃₄N₂OPS: C 81.36, H 4.42, N 3.72, S 4.26; found: C 81.38, H 4.37, N 3.71, S 5.31.

Results and Discussion

Synthesis

The synthetic route for compound **PhImPOTD** is outlined in Scheme 1. The detailed procedures for the syntheses of the reaction intermediates and final products are depicted in synthesis part. **PhImPOTD** is composed of three main

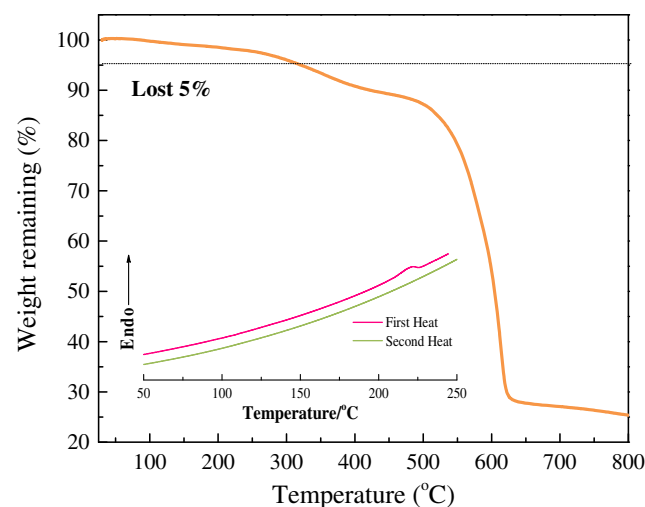
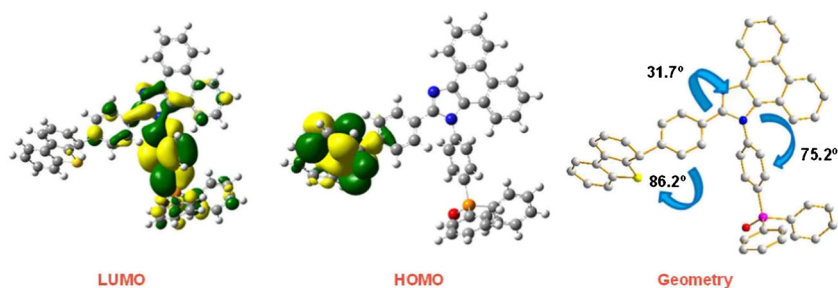


Fig. 1 TGA thermogram of **PhImPOTD** (at 10 °C min⁻¹ under nitrogen atmosphere). Inset: Differential scanning calorimetry (DSC) spectrum of the first and second heating cyclings for **PhImPOTD** at a heating rate of 10 °C min⁻¹ under nitrogen flushing

Fig. 2 The optimized molecular geometries of **PhImPOTD** calculated with DFT on a B3LYP/6-31G(d) level



components: **PI** as the acceptor moiety, dibenzothiophene as the donor moiety and diphenylphosphine oxide as the branch of phenathroimidazole. Firstly, **TD4B** is successively achieved by bromination and borate acidification of dibenzothiophene at C-4 positions. Secondly, the diphenylphosphine oxide (**PO**) group is not directly treated with deprotonation for the NH group on imidazole. We chose the moderate synthetic route to construct 4-(diphenylphosphinyl)benzenamine by zinc and nickel co-catalysis. The key backbone **PhImPOBr** is prepared by one-pot cyclizing reaction with high yields. This synthesis method could conveniently construct **PI** derivatives with various structures by tuning aromatic aldehyde and primary amine [32]. The target molecule is obtained through the typical Suzuki-Miyaura cross-coupling reactions between the bromide intermediate **PhImPOBr** and the boronic ester **TD4B** catalyzed by Pd(PPh₃)₄-NaOH in 64% yields. In order to pursue the maximized yields, the selective aprotic solvents THF, toluene and 1,4-dioxane were utilized for this reaction. The results prove that the utilization of THF can be apt to the maximized yields. The identity of **PhImPOTD** is fully characterized by standard spectroscopic techniques, which gives satisfactory analysis data corresponding to chemical structure and demonstrates its high purity. **PhImPOTD** has

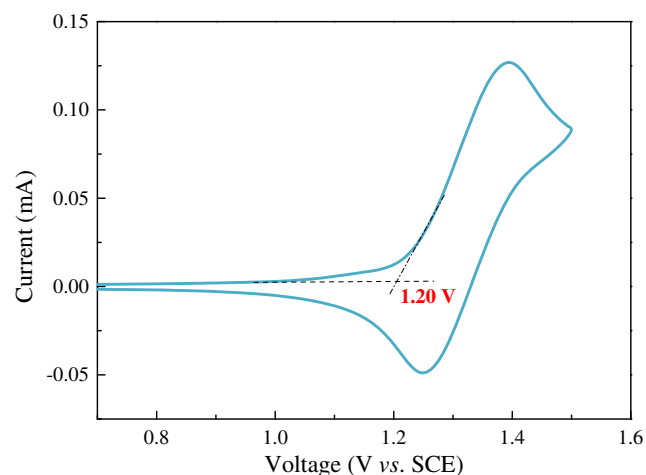


Fig. 3 Cyclic voltammogram of **PhImPOTD**. In each case, the anodic scan was performed in CH₂Cl₂ at a scan rate of 100 mV s⁻¹. The working electrode: platinum wire; the auxiliary electrode: platinum wire with a porous ceramic wick; the reference electrode: calomel electrode

good solubility in common organic solvents such as THF, dichloromethane, chloroform and toluene.

Thermal Properties

The thermal properties of **PhImPOTD** are examined by thermogravimetric analysis (TGA) and differential scanning calorimetry (DSC) measurements, as shown in Fig. 1. **PhImPOTD** shows good thermal stability, which is indicated by high decomposition temperature (T_d , corresponding to 5% weight loss) of 321 °C. Such value is ca. 60 °C higher than **PI** unit ($T_d = 262$ °C). In addition, no phase transition, like the glass transition and the melting temperature, is observed in the tested temperature range, indicating the noncrystalline or amorphous characteristics of **PhImPOTD** [33]. The nonplanar **PO** and **TD** units in molecule hinder close packing, which is beneficial for the formation of amorphous thin film by vacuum deposition.

Theoretical Calculations and Electrochemical Properties

To gain further insight into the structure-property relationship, we performed the geometry optimization of **PhImPOTD** using the DFT calculations with the Gaussian 09 series of programs using the B3LYP hybrid functional and 6-31G(d)

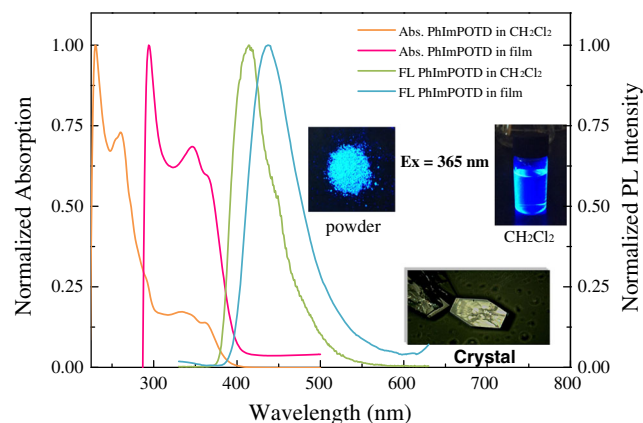


Fig. 4 Normalized absorption spectra and fluorescence spectra of **PhImPOTD** in CH₂Cl₂ at 10⁻⁶ M and in spin-coating film on a quartz plate at 298 K, respectively. Inset: photographs of **PhImPOTD** in CH₂Cl₂ and in the solid state under 365 nm hand-lamp irradiation; photographs of single crystal captured through optical microscope

Table 1 The photophysical and thermal properties of **PhImPOTD**

	$\lambda_{\max, \text{abs}}/\text{nm}^a$	$\lambda_{\max, \text{PL}}/\text{nm}^a$	$\lambda_{\max, \text{film}}/\text{nm}^b$	PLQY _{solution} ^a	PLQY _{film} ^b	Tg/°C ^c	Td/°C ^d	HOMO/eV ^e	LUMO/eV ^f	E _g /eV ^g
PhImPOTD	230, 260, 339	414	438	0.62	0.34	–	321	5.60	2.41	3.19

^a Measured in CH₂Cl₂ solution at room temperature^b Measured in spin-coating film at room temperature^c Tg: glass transition temperature, obtained from DSC measurements^d Td: decomposition temperature at weight loss of 5 %, obtained from TGA measurements^e HOMO was calculated from the onset value of the oxidation potential^f LUMO was calculated from the HOMO and the optical band gap E_g^g E_g: the optical band gap was calculated from the absorption spectra

basis set. Figure 2 presents the distributions of the frontier molecular orbitals (FMO), i.e., the highest occupied molecular orbital (HOMO) and the lowest unoccupied molecular orbital (LUMO). The HOMOs are situated on the dibenzothiophene unit, while the LUMOs are mainly localized on the imidazole, diphenylphosphine oxide group and the linker phenyl segments due to the inductive effect of P = O. It is noteworthy that with a most twisted conformation due to **TD** at the 4-position of **PI**, it brings about the separated HOMO and LUMO level distribution localized on the D and A moieties, which indicates that HOMO–LUMO excitation would shift the electron density distribution from one side of the **TD** groups as the donor to the other side **PI** as the acceptor. These observations are in accord with the fact that **TD** is a hole transport unit and **PI** is an electron transport unit for **PhImPOTD**. It is more important, such separation of HOMO and LUMO can provide hole- and electron-transporting channel respectively. Moreover, the dihedral angles between the adjacent phenyl linker and **PI** are 31.7°. The dihedral angles between the imidazole and deprotonation group are 75.2°. Closer inspection reveals the conjugated phenyl linker and the adjacent **TD** plane intersect with the

approximately perpendicular dihedral angles of 86.2°. The twisted conformation brings out the less overlapped spatial distributions of the HOMO and LUMO, which is beneficial to charge balance and exciton recombination in devices.

The experimental LUMO and HOMO energy levels of **PhImPOTD** was estimated with cyclic voltammetry (CV), as shown in Fig. 3. **PhImPOTD** shows a single irreversible oxidation peak with the similar onset voltages around 1.20 eV, corresponding to the HOMO energy levels of –5.60 eV (assuming that the absolute energy level of the Fc/Fc⁺ redox couple was 4.40 eV below vacuum). The energy level of LUMO was calculated by using Eqs. (3) and (4):

$$E_g = 1240 / \lambda_{\text{onset}} \quad (3)$$

$$E_{\text{LUMO}} = E_{\text{HOMO}} + E_g \quad (4)$$

The corresponding LUMO energy level of **PhImPOTD** was calculated to be –2.41 eV. The molecular orbital data indicate that the HOMO/LUMO level of diphenylphosphine oxide substituted **PhImPOTD** are obviously lower than

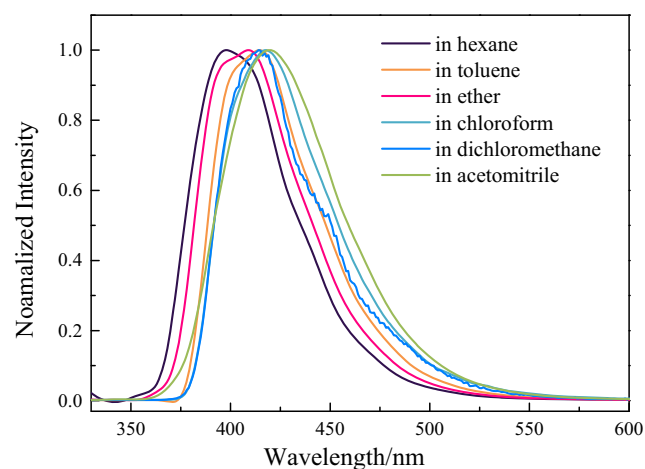
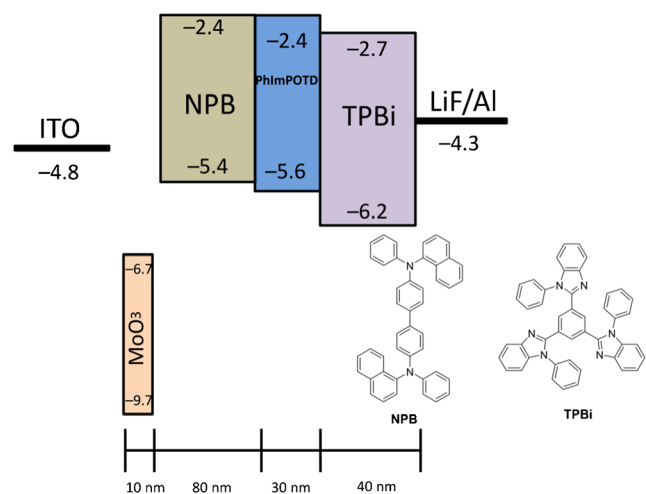
**Fig. 5** Solvatochromic shifts of PL spectra of **PhImPOTD****Scheme 2** Energy level of device A and chemical structures of the carrier transporting materials

Table 2 Key performance parameters of non-doped deep blue devices

Material	Device	V_{on} (V) ^a	λ_{max} (nm)	FWHM (nm)	CE_{max}^b (cd A ⁻¹)	PE_{max}^b (lm W ⁻¹)	EQE_{max}^b (%)	CIE (x, y) ^c
PhImPOTD	A	3.6	444	62	1.13	0.50	1.00	(0.151, 0.084)
PhImPOTD + PO01	B	3.6	444 + 556	–	4.83	2.15	2.2	(0.317, 0.315)

^a Voltage required for 1 cd m⁻²

^b current efficiency (CE_{max}), power efficiency (PE_{max}), external quantum yield (EQE_{max})

^c The CIE are measured at 1000 cd m⁻²

those of the electron-rich substituted one [28], which proved the electrophilic substituent group pulls the HOMO/LUMO levels down.

Photophysical Properties

The electronic absorption and steady-state photoluminescence spectra of **PhImPOTD** were measured at room temperature in dichloromethane and in thin film, as illustrated in Fig. 4 and Table 1. The compound features the intense absorption bands in the region of 230–390 nm in dichloromethane, which consist of three bands around 230, 260 and 339 nm. The strong absorption peak located at 230 nm originated from the $\pi \rightarrow \pi^*$ transition of diphenylphosphinyl moiety [34]. The absorption bands at around 260 nm can be assigned to the isolated benzene ring connected with imidazole [35], the $\pi \rightarrow \pi^*$ transition of dibenzothiophene (280–305 nm) partially merges with this absorption band, the broad absorption bands at 339 nm might be corresponds to the $\pi-\pi^*$ transition of the substituent on the 2-imidazole position to the **PI** unit [36]. Moreover, the optical gap in solution was 3.19 eV for **PhImPOTD**, estimated according to the onset of the absorption spectrum in CH₂Cl₂. In the photoluminescence spectra, **PhImPOTD** shows a structureless emission peak at 414 nm. As expected, the emission maxima of **PhImPOTD** in a thin film (at 438 nm) is bathochromic shifted by ca. 24 nm in comparison

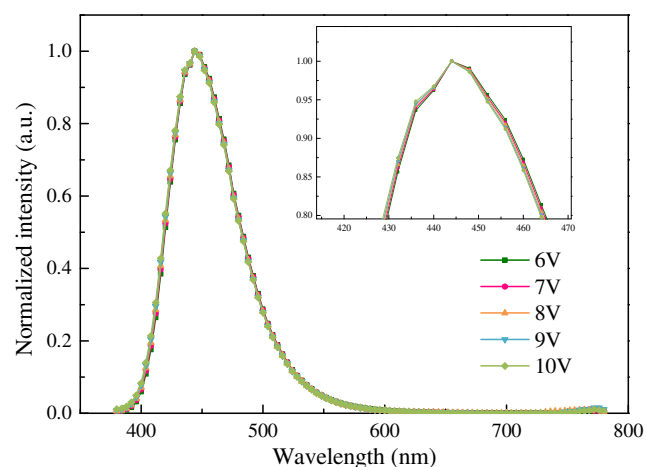


Fig. 6 Electroluminescence spectra for device A at different voltages. The inset shows a magnified view of the emission peaks

with that in solution, which is likely to be caused by $\pi-\pi$ stacking and intermolecular aggregation in the solid state. The photoluminescence quantum yield (PLQY) is determined by 9,10-diphenylanthracene ($\Phi = 0.9$ in cyclohexane) as a standard. **PhImPOTD** shows the PLQY is as high as 0.62 in CH₂Cl₂. However, PLQY is decreased to 0.34 in the solid state, which should be attributed by the aggregation quenching. Then, the solvatochromic shifts are investigated in different polarity solvents. These solvents are *n*-hexane, toluene, chloroform, ether, dichloromethane and acetonitrile, respectively. The orientation polarization of these solvents are 0.0012, 0.014, 0.15, 0.17, 0.22 and 0.31, respectively. The emission colors obtained from various solutions, and solvatochromic shifts of PL spectra for **PhImPOTD** are shown in Fig. 5. The wavelength of maximum PL intensity for **PhImPOTD** red-shifted from 398 (*n*-hexane) to 420 nm (acetonitrile), with increasing solvent polarity. Such solvatochromic behavior demonstrates the existence of CT moiety in the excited state [37].

Electroluminescence Properties

To explore the EL properties of **PhImPOTD**, we construct the device A with a frequently used multilayered structure: indium tin oxide (ITO)/MoO₃ (10 nm)/ *N,N'*-Bis-(1-naphthalenyl)-*N,N'*-bis-phenyl-(1,1'-biphenyl)-4,4'-diamine (NPB) (80 nm)/ **PhImPOTD** (30 nm)/ 1,3,5-Tri(1-phenyl-1H-benzo[*d*]imidazol-2-yl)phenyl (TPBi) (40 nm)/LiF (1 nm)/Al

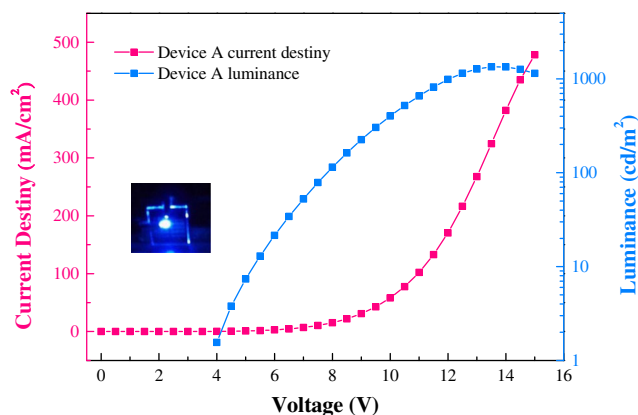


Fig. 7 Current density–voltage–luminance characteristics for devices A

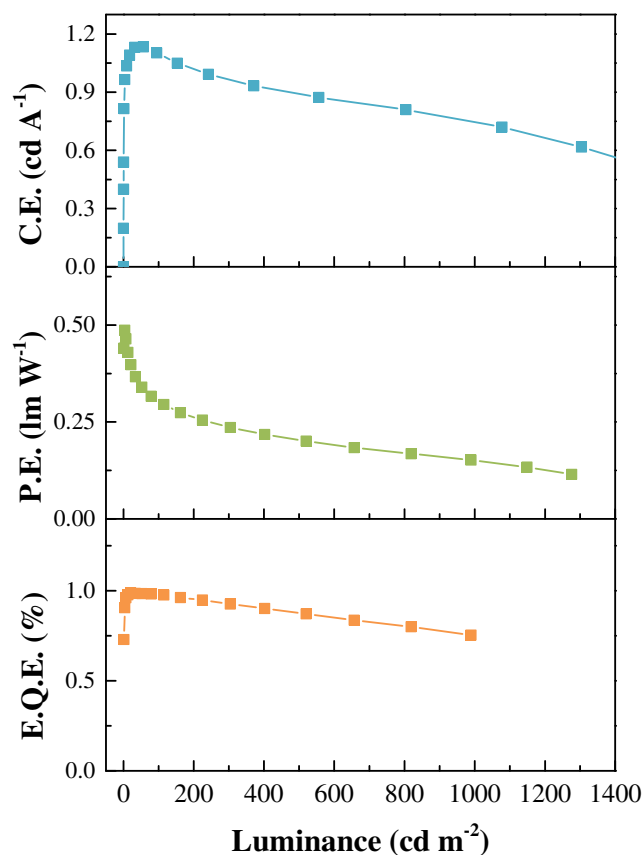


Fig. 8 Efficiency versus luminance curves of non-doped blue device based on **PhImPOTD**

(100 nm), in which MoO_3 and LiF are utilized as a hole and an electron-injecting layer, respectively. NPB and TPBi serve as a hole and an electron-transporting layer, respectively (Scheme 2). The key parameters of device are summarized in Table 2. From the EL spectra, shown in Fig. 6, we could see an obvious deep-blue emission with λ_{max} at 444 nm and

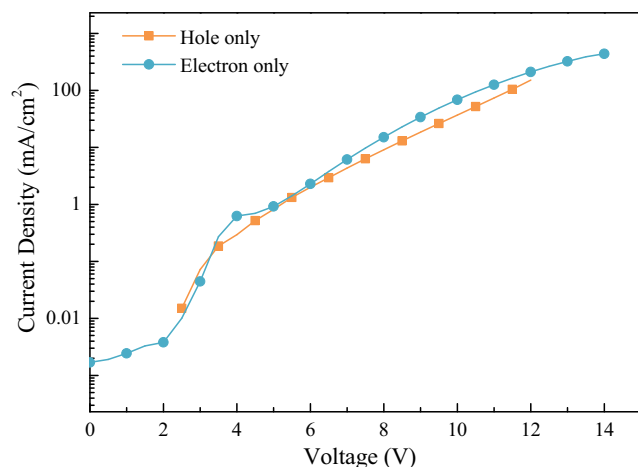


Fig. 9 Current density versus voltage characteristics of hole-only and electron-only devices for **PhImPOTD**

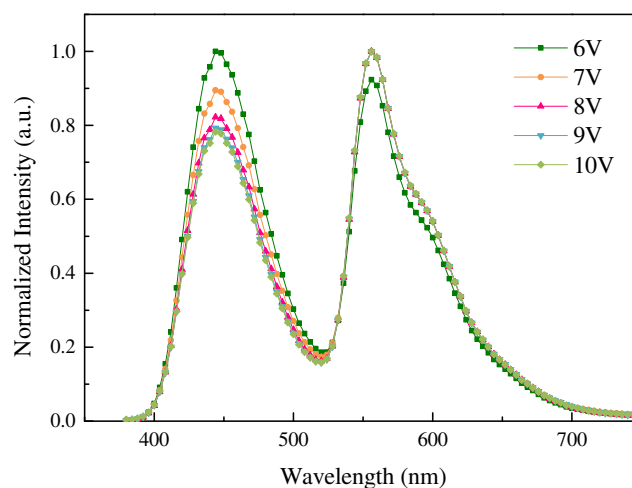


Fig. 10 Electroluminescence spectra for device B at different voltages

no vibronic feature under the applied voltages ranging from 6 to 10 V. Evidently, such the EL spectrum is very similar to the PL spectra observed from film. In detail, the full width at half maximum (FWHM) of EL and PL is 62 nm and 68 nm, respectively. Noticeably, no other emission from any other layers was observed for device A, suggesting that all excitons generated in the device are effectively confined in the emitting layer (EML). At the same time, no excimer or exciplex emission was observed. Due to the substituent on the imidazole position and the polyaromatic hydrocarbon moieties, **PhImPOTD** exists the locally twisted structure, which results in large steric hindrance. Figure 7 and Fig. 8 show the current density-voltage-luminance (J - V - L) characteristics and plots of efficiency versus current density of the fabricated deep blue device, respectively. The device yields a maximum luminance of 1341 cd m^{-2} , an external quantum yield of 1.00%, and a maximum luminous efficiency of 1.13 cd A^{-1} . Despite the efficiencies of device with **PhImPOTD** are slightly lower than those of the reference devices [28, 36], it is definitely a worthwhile work that Commission Internationale de l'Éclairage (CIE) color coordinates of (0.15, 0.08) are

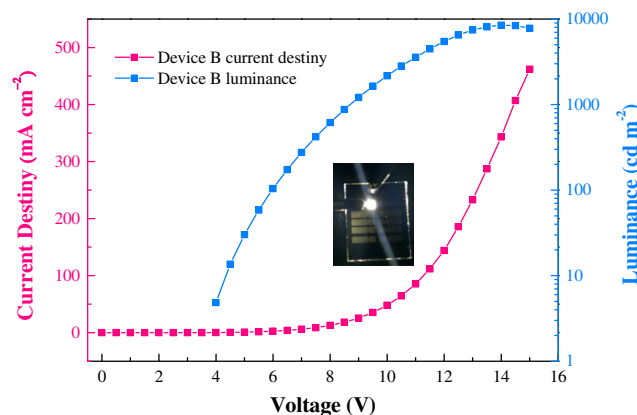


Fig. 11 Current density-voltage-luminance characteristics for device B

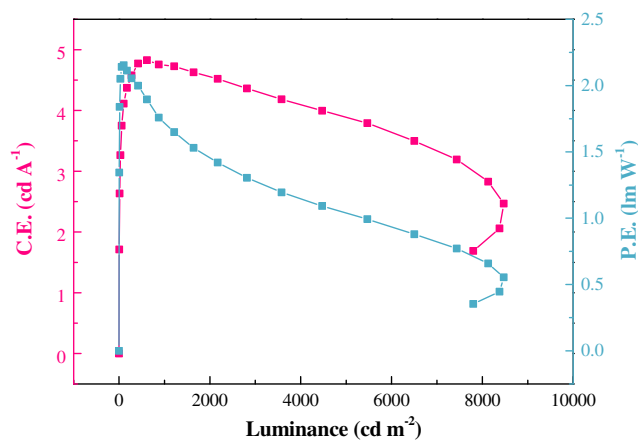


Fig. 12 Efficiency versus luminance curves of doped white device B based on **PhImPOTD**

attained. This value is very close to the NTSC (National Television Standards Committee) blue standard (CIE: 0.14, 0.08). Meanwhile, the device A shows low turn-on voltage of 3.6 V, which should be attributed to the well matched HOMO level of diphenylphosphine substituent **PI** emitters (5.6 eV) and the adjacent NPB (5.4 eV). To further understand the charge injection/transportation characteristics of **PhImPOTD**, we fabricated the single-carrier devices with the configurations of ITO/MoO₃ (0.2 nm)/NPB (40 nm)/**PhImPOTD** (30 nm)/NPB (40 nm)/MoO₃ (0.2 nm)/Al (100 nm) (hole-only transporting device) and ITO/LiF (0.1 nm)/TPBi (40 nm)/**PhImPOTD** (30 nm)/TPBi (40 nm)/LiF (0.1 nm)/Al (100 nm) (electron-only transporting device). MoO₃ and TPBi layers are used to prevent electron and hole injection from the cathode and anode, respectively. As depicted in Fig. 9, the current density–voltage (*J*–*V*) characteristics illustrate that the hole current density values of **PhImPOTD** approximate the same as the electron current density, which undoubtedly evidences the balanced bipolar charge transport capacity of **PhImPOTD**. All these results indicate that **PhImPOTD** is an excellent bipolar material, which can be served as non-doped deep blue OLEDs.

WOLEDs have drawn tremendous intentions and been studied extensively because of their great promise for universal application in future solid-state lighting sources and backlights for full-color displays [38]. White-light emission can be acquired by complementary color (blue plus yellow or blue, green plus red) or broadband emission. To further explore the potential of deep blue emitter **PhImPOTD** [39, 40], we tried to fabricate device B through precisely controlling the ratio of **PhImPOTD** and the complementary yellow emitter PO-01 (acetylacetonatobis(4-phenylthieno[3,2-*c*]pyridinato-*N,C2'*) Iridium), aiming for achieving WOLEDs. The typical EL spectra of the WOLEDs at different voltages are shown in Fig. 10. The dual emissions EL spectra could be divided into their blue emission (444 nm) corresponding to the fluorophore **PhImPOTD** and yellow emission (556 nm) corresponding to

the phosphor PO-01. The low driving voltage of 3.6 V for onset is realized owing to the well matching HOMO/LUMO level between EML and transport layers. (Fig. 11). **PhImPOTD** and PO-01 endow device B the high efficiencies with 4.83 cd A⁻¹ for maximum current efficiency (C.E.), 2.15 lm W⁻¹ for power efficiency (P.E.) and a maximum luminance of 8472 cd m⁻² (Fig. 12). The white light emitting device is with the CIE coordinates of (0.32, 0.32) at the luminance of 1000 cd m², which is very close to the standard white light point of (0.33, 0.33). In addition, a small offset of CIE coordinates of emitted light is observed under the various biases (at the luminance of 300–7500 cd A⁻¹), which reflects good color stability for doped WOLEDs. The inset of Fig. 11 is a snapshot of the WOLED at 14.0 V; a suitable white light emission with a uniform emitting area is seen.

Conclusion

In summary, a new phenanthroimidazole derivative **PhImPOTD** with ambipolar transport behavior has been synthesized and characterized. By combing the advantages of phenanthroimidazole backbone and the D– π –A structure, high efficient deep blue emitter was achieved. Further, the deprotonation of *n*-type imidazole moiety by electron-withdrawing diphenylphosphine oxide increased the unsymmetrical configuration, which could efficiently prevent the strong π – π stacking and molecular interactions. It is reasonable that **PhImPOTD** possesses high quantum efficiency and thermal stability. **PhImPOTD** has not only been used as emitter to fabricate deep-blue OLEDs, but also as host materials to construct highly efficient WOLEDs. Non-doped **PhImPOTD** multilayer device exhibits a deep-blue emission (CIE: 0.15, 0.08), together with a low driving voltage of 3.6 V, efficiencies of 1.13 cd A⁻¹ for C.E., and 1.00% for E.Q.E. Doped WOLED with CIE coordinates of (0.32, 0.32) gave the performance of 4.83 cd A⁻¹ for C.E., 2.15 lm W⁻¹ for P.E. and 3.6 V for onset voltage. It also possesses good color stability under broad luminance. We believe that this work gives a novel clue for high performance deep blue and white emitting fluorescent OLEDs.

Acknowledgements The authors are grateful for the support by National Natural Science Foundation of China (Grant No. 111572002) and the Foundation for Innovative Research Groups of the National Natural Science Foundation of China (Grant No. 11521202).

References

1. Lee CW, Lee JY (2013) Above 30% external quantum efficiency in blue phosphorescent organic light-emitting diodes using pyrido[2,3-*b*]indole derivatives as host materials. *Adv Mater* 25:5450–5454

2. Liu Z, Qi W, Xu G (2015) Recent advances in electrochemiluminescence. *Chem Soc Rev* 44:3117–3142
3. Lee CW, Lee JY (2015) Systematic control of photophysical properties of host materials for high quantum efficiency above 25% in green thermally activated delayed fluorescent devices. *ACS Appl Mater Interfaces* 7:2899–2904
4. Lee DR, Hwang SH, Jeon SK, Lee CW, Lee JY (2015) Benzofurocarbazole and benzothienocarbazole as donors for improved quantum efficiency in blue thermally activated delayed fluorescent devices. *Chem Commun* 51:8105–8107
5. Choy WC, Chan WK, Yuan Y (2014) Recent advances in transition metal complexes and light-management engineering in organic optoelectronic devices. *Adv Mater* 26:5368–5398
6. Hung WY, Chiang PY, Lin SW, Tang WC, Chen YT, Liu SH, Chou PT, Hung YT, Wong KT (2016) Balance the carrier mobility to achieve high performance exciplex OLED using a triazine-based acceptor. *ACS Appl Mater Interfaces* 8:4811–4818
7. Hatakeyama T, Shiren K, Nakajima K, Nomura S, Nakatsuka S, Kinoshita K, Ni J, Ono Y, Ikuta T (2016) Ultrapure blue thermally activated delayed fluorescence molecules: efficient HOMO–LUMO separation by the multiple resonance effect. *Adv Mater* 28:2777–2781
8. Ivaniuk K, Cherpak V, Stakhira P, Hotra Z, Minaev B, Baryshnikov G, Stroylyo E, Volyniuk D, Grazulevicius JV, Lazauskas A, Tamulevicius S, Witulski B, Light ME, Gawrys P, Whitby RJ, Wiosna-Salyga G, Luszczynska B (2016) Highly luminous sky-blue organic light-emitting diodes based on the bis[(1,2)(5,6)]indoloanthracene emissive layer. *J Phys Chem C* 120:6206–6217
9. Lee J, Chen HF, Batagoda T, Coburn C, Djurovich PI, Thompson ME, Forrest SR (2016) Deep blue phosphorescent organic light-emitting diodes with very high brightness and efficiency. *Nat Mater* 15:92–98
10. Gong S, Yang C, Qin J (2012) Efficient phosphorescent polymer light-emitting diodes by suppressing triplet energy back transfer. *Chem Soc Rev* 41:4797–4807
11. Volz D, Wallesch M, Fléchon C, Danz M, Verma A, Navarro JM, Zink DM, Bräse S, Baumann T (2015) From iridium and platinum to copper and carbon: new avenues for more sustainability in organic light-emitting diodes. *Green Chem* 17:1988–2011
12. Lee J, Park J (2015) Synthesis and electroluminescence of novel pyrene-fused chromophores. *Org Lett* 17:3960–3963
13. Kim JB, Han SH, Yang K, Kwon SK, Kim JJ, Kim YH (2015) Highly efficient deep-blue phosphorescence from heptafluoropropyl-substituted iridium complexes. *Chem Commun* 51:58–61
14. Huang J, Sun N, Chen P, Tang R, Li Q, Ma D, Li Z (2014) Largely blue-shifted emission through minor structural modifications: molecular design, synthesis, aggregation-induced emission and deep-blue OLED application. *Chem Commun* 50:2136–2138
15. Hua W, Liu Z, Duan L, Dong G, Qiu Y, Zhang B, Cui D, Tao X, Cheng N, Liu Y (2015) Deep-blue electroluminescence from nondoped and doped organic light-emitting diodes (OLEDs) based on a new monoaza[6]helicene. *RSC Adv* 5:75–84
16. Lee J, Kim B, Kwon JE, Kim J, Yokoyama D, Suzuki K, Nishimura H, Wakamiya A, Park SY, Park J (2014) Excimer formation in organic emitter films associated with a molecular orientation promoted by steric hindrance. *Chem Commun* 50:14145–14148
17. Han C, Zhang Z, Xu H, Li J, Xie G, Chen R, Zhao Y, Huang W (2012) Controllably tuning excited-state energy in ternary hosts for ultralow-voltage-driven blue electrophosphorescence. *Angew Chem Int Ed* 51:10104–10108
18. Tao Y, Xiao J, Zheng C, Zhang Z, Yan M, Chen R, Zhou X, Li H, An Z, Wang Z, Xu H, Huang W (2013) Dynamically adaptive characteristics of resonance variation for selectively enhancing electrical performance of organic semiconductors. *Angew Chem Int Ed* 52:10491–10495
19. Zhang Y, Lai SL, Tong QX, Lo MF, Ng TW, Chan MY, Wen ZC, He J, Jeff KS, Tang XL, Liu WM, Ko CC, Wang PF, Lee CS (2012) High efficiency nondoped deep-blue organic light emitting devices based on imidazole- π -triphenylamine derivatives. *Chem Mater* 24:61–70
20. Wang K, Zhao F, Wang C, Chen S, Chen D, Zhang H, Liu Y, Ma D, Wang Y (2013) High-performance red, green, and blue electroluminescent devices based on blue emitters with small singlet–triplet splitting and ambipolar transport property. *Adv Funct Mater* 23:2672–2680
21. Li W, Liu D, Shen F, Ma D, Wang Z, Feng T, Xu Y, Yang B, Ma Y (2012) A twisting donor-acceptor molecule with an intercrossed excited state for highly efficient, deep-blue electroluminescence. *Adv Funct Mater* 22:2797–2803
22. Chou HH, Chen YH, Hsu HP, Chang WH, Chen YH, Cheng CH (2012) Synthesis of diimidazolylstilbenes as n-type blue fluorophores: alternative dopant materials for highly efficient electroluminescent devices. *Adv Mater* 24:5867–5871
23. Lee W, Yang Y, Cho N, Ko J, Hong JI (2012) Functionalized organic dyes containing a phenanthroimidazole donor for dye-sensitized solar cell applications. *Tetrahedron* 68:5590–5598
24. Wang ZM, Song XH, Gao Z, Yu DW, Zhang XJ, Lu P, Shen FZ, Ma YG (2012) Tuning of the electronic and optical properties of 4,4'-bis(1-phenylphenanthro[9,10-d]imidazol-2-yl)biphenyl via cyano substitution in un-conjugated phenyl. *RSC Adv* 2:9635–9642
25. Zhuang S, Shangguan R, Jin J, Tu G, Wang L, Chen J, Ma D, Zhu X (2012) Efficient nondoped blue organic light-emitting diodes based on phenanthroimidazole-substituted anthracene derivatives. *Org Electron* 13:3050–3059
26. Gao Z, Liu Y, Wang Z, Shen F, Liu H, Sun G, Yao L, Lv Y, Lu P, Ma Y (2013) High-efficiency violet-light-emitting materials based on phenanthro[9,10-d]imidazole. *Chem Eur J* 19:2602–2605
27. Huang H, Wang Y, Wang B, Zhuang S, Pan B, Yang X, Wang L, Yang C (2013) Controllably tunable phenanthroimidazole–carbazole hybrid bipolar host materials for efficient green electrophosphorescent devices. *J Mater Chem C* 1:5899–5908
28. Chen S, Wu Y, Zhao Y, Fang D (2015) Deep blue organic light-emitting devices enabled by bipolar phenanthro[9,10-d]imidazole derivatives. *RSC Adv* 5:72009–72018
29. Frisch MJ, Trucks GW, Schlegel HB, Scuseria GE, Robb MA, Cheeseman JR, Scalmani G, Barone V, Mennucci B, Petersson GA, Nakatsuji H, Caricato M, Li X, Hratchian HP, Izmaylov AF, Bloino J, Zheng G, Sonnenberg JL, Hada M, Ehara M, Toyota K, Fukuda R, Hasegawa J, Ishida M, Nakajima T, Honda Y, Kitao O, Nakai H, Vreven T, Montgomery Jr JA, Peralta JE, Ogliaro F, Bearpark M, Heyd JJ, Brothers E, Kudin KN, Staroverov VN, Kobayashi R, Normand J, Raghavachari K, Rendell A, Burant JC, Iyengar SS, Tomasi J, Cossi M, Rega N, Millam JM, Klene M, Knox JE, Cross JB, Bakken V, Adamo C, Jaramillo J, Gomperts R, Stratmann RE, Yazyev O, Austin AJ, Cammi R, Pomelli C, Ochterski JW, Martin RL, Morokuma K, Zakrzewski VG, Voth GA, Salvador P, Dannenberg JJ, Dapprich S, Daniels AD, Farkas Ö, Foresman JB, Ortiz JV, Cioslowski J, Fox DJ (2009) Gaussian 09, revision A02. Gaussian, Inc, Wallingford CT
30. Becke AD (1993) Density-functional thermochemistry. III the role of exact exchange. *J Chem Phys* 98:5648–5652
31. Lee C, Yang W, Parr RG (1988) Development of the Colle-Salvetti correlation-energy formula into a functional of the electron density. *Phys Rev B* 37:785–789
32. Yuan Y, Chen JX, Lu F, Tong QX, Yang QD, Mo HW, Ng TW, Wong FL, Guo ZQ, Ye J, Chen Z, Zhang XH, Lee CS (2013) Bipolar phenanthroimidazole derivatives containing bulky polyaromatic hydrocarbons for nondoped blue electroluminescence

- devices with high efficiency and low efficiency roll-off. *Chem Mater* 25:4957–4965
33. Qin W, Yang Z, Jiang Y, Lam JWY, Liang G, Kwok HS, Tang BZ (2015) Construction of efficient deep blue aggregation-induced emission luminogen from triphenylethene for nondoped organic light-emitting diodes. *Chem Mater* 27:3892–3901
 34. Fan C, Duan C, Wei Y, Ding D, Xu H, Huang W (2015) Dibenzothiophene-based phosphine oxide host and electron-transporting materials for efficient blue thermally activated delayed fluorescence diodes through compatibility optimization. *Chem Mater* 27:5131–5140
 35. Gao Z, Cheng G, Shen F, Zhang S, Zhang Y, Lu P, Ma Y (2014) Highly efficient deep blue light emitting devices based on triphenylsilane modified phenanthro[9,10-d]imidazole. *Laser Photonics Rev* 8:L6–L10
 36. Gao Z, Wang Z, Shan T, Liu Y, Shen F, Pan Y, Zhang H, He X, Lu P, Yang B, Ma Y (2014) High-efficiency deep blue fluorescent emitters based on phenanthro[9,10-d]imidazole substituted carbazole and their applications in organic light emitting diodes. *Org Electron* 15:2667–2676
 37. Tanaka H, Shizu K, Lee J, Adachi C (2015) Effect of atom substitution in chalcogenodiazole-containing thermally activated delayed fluorescence emitters on radiationless transition. *J Phys Chem C* 119:2948–2955
 38. Farinola GM, Ragni R (2011) Electroluminescent materials for white organic light emitting diodes. *Chem Soc Rev* 40:3467–3482
 39. Peng T, Yang Y, Bi H, Liu Y, Hou Z, Wang Y (2011) Highly efficient white organic electroluminescence device based on a phosphorescent orange material doped in a blue host emitter. *J Mater Chem* 21:3551–3553
 40. Chen Z, Liu XK, Zheng CJ, Ye J, Liu CL, Li F, Ou XM, Lee CS, Zhang XH (2015) High performance exciplex-based fluorescence – phosphorescence white organic light-emitting device with highly simplified structure. *Chem Mater* 27:5206–5211